Atmos. Meas. Tech. Discuss., 7, 6529–6564, 2014
www.atmos-meas-tech-discuss.net/7/6529/2014/
doi:10.5194/amtd-7-6529-2014

Atmospheric Measurement Techniques Discussions
Open Access

High precision dual-inlet IRMS measurements of the stable isotopes of CO_2 and the N_2O/CO_2 ratio from polar ice core samples

T. K. Bauska, E. J. Brook, A. C. Mix, and A. Ross

College of Earth, Ocean and Atmospheric Sciences, Oregon State University, Corvallis, OR 97331, USA

Received: 3 April 2014 – Accepted: 11 June 2014 – Published: 3 July 2014

Correspondence to: T. K. Bauska (bauskat@geo.oregonstate.edu)

Published by Copernicus Publications on behalf of the European Geosciences Union.

Abstract

An important constraint on mechanisms of past carbon cycle variability is provided by the stable isotopic composition of carbon in atmospheric carbon dioxide (δ^{13}C-CO_2) trapped in polar ice cores, but obtaining very precise measurements has proven to be a significant analytical challenge. Here we describe a new technique to determine the δ^{13}C of CO_2 at exceptional precision, as well as measuring the CO_2 and N_2O mixing ratios. In this method, ancient air is extracted from relatively large ice samples (~ 400 grams) with a dry-extraction "ice-grater" device. The liberated air is cryogenically purified to a CO_2 and N_2O mixture and analyzed with a micro-volume equipped dual-inlet IRMS (Thermo MAT 253). The reproducibility of the method, based on replicate analysis of ice core samples, is 0.02 ‰ for δ^{13}C-CO_2 and 2 ppm and 4 ppb for the CO_2 and N_2O mixing ratios, respectively (1-sigma pooled standard deviation). Our experiments show that minimizing water vapor pressure in the extraction vessel by housing the grating apparatus in a ultra-low temperature freezer (−60 °C) improves the precision and decreases the experimental blank of the method. We describe techniques for accurate calibration of small samples and the application of a mass spectrometric method based on source fragmentation for reconstructing the N_2O history of the atmosphere. The oxygen isotopic composition of CO_2 is also investigated, confirming previous observations of oxygen exchange between gaseous CO_2 and solid H_2O within the ice archive. These data offer a possible constraint on oxygen isotopic fractionation during H_2O and CO_2 exchange below the H_2O bulk melting temperature.

1 Introduction

The air occluded in polar ice is an outstanding archive of the ancient atmosphere. Over the past few decades, highly specialized analytical methods have yielded excellent records of climate and biogeochemical processes. Measuring trace gases from ice core samples presents a number of significant technical challenges, most notably

AMTD
7, 6529–6564, 2014

how to extract the air from the ice without significantly altering the in situ composition, and how to make accurate and precise measurements on limited amounts of air. Many current ice core δ^{13}C-CO_2 methods have precision of about 0.1 ‰ (see below). This limits interpretation of mechanisms because the uncertainty is about 1/3 of the full dynamic range observed on glacial-interglacial timescales (~ 0.3 ‰) (Schmitt et al., 2012). Additionally, fluxes of carbon depleted in ^{13}C from the terrestrial biosphere (~ −25 ‰) on decadal to centennial timescales leave an isotopic imprint on the atmosphere (~ 6.5 ‰) of about -0.03 ‰ ppm^{-1} CO_2 (after exchange with the oceanic reservoir) (Trudinger et al., 2002). With modern atmospheric measurements capable of precision of 0.01 ‰ (Masarie et al., 2001), improvements in ice core methods have huge potential to constrain paleo-atmospheric isotopic budgets and the mechanisms of CO_2 variability.

Early efforts to analyze carbon isotope ratios of CO_2 in ice cores using milling devices on large samples with dual-inlet IRMS measurements obtained precisions of about 0.1 ‰ (Friedli and Stauffer, 1986; Leuenberger et al., 1992). Subsequently, dual-inlet IRMS measurements improved the constraints on the Last Glacial termination and Holocene history (Indermuhle et al., 1999; Smith et al., 1999) but precision remained about 0.08 ‰. More recently, gas-chromatographic IRMS (GC-IRMS) methods have significantly decreased the required sample size, which allows for greater sampling resolution and simpler mechanical crushers. However, precision with these techniques is still about 0.1 ‰ (Elsig et al., 2009; Leuenberger et al., 2003; Lourantou et al., 2010; Schaefer et al., 2011). A novel method that employs sublimation to release the occluded air followed by GC-IRMS measurement techniques has made significant improvement to the precision obtained from small samples (0.05–0.09 ‰) (Schmitt et al., 2011). The highest precision measurements (0.025–0.05 ‰) to date were obtained from the Law Dome ice core spanning the last millennium using an large volume ice grater and dual-inlet technique (Francey et al., 1999). However, this record was recently augmented and revised to account for a significant shift in the mean values of many of the measurements. When an estimate of changing accuracy was included, the

AMTD
7, 6529–6564, 2014

average uncertainty for individual measurements was similar to that of other methods, about 0.06 ‰ (Rubino et al., 2013).

Due to the limited availability of ice samples, many methods are designed to minimize sample consumption at the expense of precision for an individual measurement. Sometimes this lower precision can be balanced by ability to collect larger numbers of replicates quickly, or to pursue higher-resolution sampling schemes. GC-IRMS techniques that require very small samples have come to dominate ice core δ^{13}C-CO_2 measurements. We approach the problem from a different perspective and aim to increase the precision of the measurement with larger samples such that fewer measurements are required to extract a low-noise signal from the ice core.

While dual-inlet IRMS typically offers better precision than GC-IRMS, it also presents two distinct problems that we address here. Firstly, N_2O interferes isobarically with CO_2. Ice core N_2O is generally atmospheric in origin, but it is occasionally produced in situ in large amounts possibly by microbial degradation of organic matter (Miteva et al., 2007). With changes in the N_2O-to-CO_2 ratio up to 30 % over a glacial–interglacial cycle, the magnitude of the δ^{13}C-CO_2 correction can range from about 0.2–0.3 ‰, introducing a systematic error. N_2O can be readily separated from CO_2 by a GC, but is practically impossible to separate from CO_2 cryogenically or in a chemically destructive manner without altering the isotopic composition of the CO_2. Dual-inlet mass spectrometry measurements thus require an accurate estimate of the N_2O-to-CO_2 ratio in the ion beam. Previous methods used to derive the N_2O-to-CO_2 ratio include: a low precision mass spectrometer method that was susceptible to experimental in situ N_2O production in the extraction apparatus (Friedli and Siegenthaler, 1988), offline measurements on an aliquot of the same sample air (Francey et al., 1999), or from an interpolation of separate data sets to the depths of the samples used for isotopic measurements (Smith et al., 1999). We utilize a method that measures the $^{14}N^{16}O$ fragment produced in the mass spectrometer source to determine the abundance and ionization efficiency of N_2O (Assonov and Brenninkmeijer, 2006). We demonstrate that

AMTD
7, 6529–6564, 2014

the method is very precise for estimating the interference correction and provides, as a byproduct, a robust record of the ice core N_2O history.

Secondly, contamination from hydrocarbon-rich drilling fluid is minimized by GC cleanup in GC-IRMS methods but could cause major problems for dual-inlet measurement if the catenated molecules, highly susceptible to fragmentation, reach the ion source. We observe that drilling fluid contamination can be effectively monitored using higher-mass detectors of high sensitivity. Along with additional cleaning steps (described below), this completely mitigates the problem in high-quality ice.

2 Ice archives

Three ice archives were utilized in this study (Table 1). The Taylor Glacier archive is a "horizontal" ice core from an ablating section of ice on the Taylor Glacier, McMurdo Dry Valleys, Antarctica (77.75° S, 161.75° E). The section encompasses a complete stratigraphic section of the last deglaciation from about 20 000 to 10 000 years before present. WDC05A is a relatively shallow depth (~ 300 m) core from the West Antarctic Ice Sheet (WAIS) Divide Ice Core Site (79.467° S, 112.085° W) and spans the last 1000 years (Mitchell et al., 2011). WDC06A is the main deep core from WAIS Divide and the data presented here span an interval from about 250–350 m (1250–750 yr B.P.).

3 Experimental procedure

3.1 Ice grater apparatus design

The ice grater extraction vessels are constructed from a stainless steel, electropolished cylinder, 25 cm in length, and capped on both ends with copper gasket sealed, 6–3/4 inch CF Flanges (Kurt Lesker Company). The flanges have been machined to remove excess weight from the exterior and bored to allow for a 3/8 inch outlet. The

AMTD
7, 6529–6564, 2014

interior of the ice grater contains a perforated stainless steel sheet, molded to form a semi-cylinder, and attached to the interior walls of the ice grater with spot welds. The perforations resemble the abrasive surface one finds on a household cheese grater used to finely grate a hard cheese.

Most of the components on the extraction line are stainless steel and are joined with either tungsten inert gas welds or copper gasket-sealed fittings (Swagelok VCR). The combination of both welds and gasket fittings lowers the chance of leaks but also maintains modularity. All the valves are bellows-sealed with spherical metal stem-tips (majority are Swagelok BG series). The pumping system is comprised of a turbo-molecular pump (Alcatel Adixen ATP 80) and scroll pump (Edwards XDS5).

During air extraction, the ice grater chamber is housed in an ultra-low temperature freezer at −60 °C (So-low, Inc.) with custom-built feed-through ports. The grater rests on an aluminum frame fixed to a linear slide apparatus, which is driven by a pneumatic piston (SG Series; PHD, Inc). A system of pneumatic valves allows the operator to control the stroke length and frequency of the motion. The pneumatic piston sits outside the freezer and the ice grater cradle slides on steel rods with teflon coated bushings. The combination of keeping the greased pneumatic piston outside of the freezer and replacing the standard lubricated ball bearings with teflon bushings proved effective in keeping the moving parts of the ice grater shaker from seizing up in the cold.

3.2 Air extraction

About 14 h prior to the first analysis, ice samples stored in a −25 °C freezer are cut and shaped with a bandsaw. The dimensions of the cut sample are typically 5 cm × 6 cm × 15 cm with masses ranging between 400 to 550 g depending on sample availability. Roughly 1–3 mm of ice from the cut surface of the sample is removed with a ceramic knife as a precautionary cleaning step.

Ice samples from coring campaigns that did not use drill fluid (WDC05A and Taylor Glacier in this study) required very minor cleaning. However, samples exposed to drilling fluid composed of HCFC-141B and Isopar-K (WDC06A in this study) required

AMTD
7, 6529–6564, 2014

an extensive cleaning procedure involving removal of about a 1 cm thickness from the exterior of the ice core piece to avoid potential micro-fractures filled with drill fluid.

After cleaning, two samples are each loaded and sealed in their respective ice grater. The graters are placed into the −60 °C freezer, attached to the extraction line (Fig. 1) via an opening in the freezer wall, and pumped to vacuum at about 0.02 Torr (in the presence of water vapor) for about 30 min. The ice graters are detached from the vacuum line, but remain sealed under vacuum in the freezer for a period of about 12 h. It is important to let the ice completely cool down because it minimizes the amount of water vapor in the extraction vessel during grating.

Prior to the sample analysis at least three aliquots of NOAA reference standard air are processed and measured like a sample, with the exception of exposure to the ice grater portion of the system (see description of air extraction below). After the initial standard runs are completed, the first chilled ice grater is reattached to the vacuum line, checked to make sure no significant leaks developed during storage, and pumped for an additional 45 min. The ice grater is then detached and placed on the pneumatic slide.

To grate the ice, the pneumatic piston drives the ice grater horizontally with a translation of 20 cm at around 2 Hz for 30 min. This is sufficient to grate about 75 % of the ice into < 1 cm diameter fragments. Typically, an ellipsoid shaped piece of about 100 grams remains intact, which can be used at a later date for additional analysis. Based on manometric measurements of the air extracted from a bubble ice sample, and typical total air content for ice (0.1 cubic centimeter per gram), the overall air extraction efficiency averages about 60 %. This is on the low end of typical dry extraction methods and an area for future improvement. Our experiments with fully and partially clathrated ice showed marked decreases in the grating efficiency (that is, the ice was still grated finely, but the piece remaining intact after a long period of time was very large), and the measurements in this type of ice were deemed too impractical for now.

After grating, the ice grater is re-coupled to the extraction line (Fig. 1). At this point, the ice grater contains about 5 Torr of sample air. A small aliquot of the sample, < 1

AMTD
7, 6529–6564, 2014

cc, is isolated from the ice grater in the extraction line (volume between Valves 1 and 15). The air sample is cyropumped through a coiled, stainless steel trap held at 170 K (with liquid nitrogen cooled ethanol) to remove water vapor and condensed at 11 K in a 7 cc sample tube held in a closed-cycle cryocooler (10K-CCR, Janis Research Company). This air sample is warmed to room temperature and stored for a few hours before being analyzed with an Agilent 7890A GC to determine the CO_2 mixing ratio. The CO_2 measurement is similar to previous methodology at Oregon State University (Ahn et al., 2009), whereby CO_2 is separated with a Porapak Q 80/100 mesh column, reduced to CH_4 with a nickel catalyst, and measured with a flame ionization detector (FID). However, whereas the previous method uses a manometer in the sample loop to determine the total air injected into the GC, we employ a thermal conductivity detector (TCD) to measure amount of O_2 and N_2 in the sample. This design minimizes the volume required for sample injection. Standard gases calibrated by NOAA on 2007 WMO Mole Fraction Scale are used to reference the sample mixing ratio (Table 2) (Zhao et al., 1997).

To extract the CO_2 and N_2O from the remaining air sample, the "w" shaped stainless steel trap is cooled with liquid nitrogen to 80 K (Fig. 1, between valves 10 and 12). Any residual non-condensible gases in the the sample air is passed over the coiled water trap (~ 170 K) and the "w" CO_2-N_2O trap (~ 80 K) by pulling the air from the ice grater through the extraction line with a turbo-molecular pump. The flow is regulated using a spherical stem-tip valve to remain less than 5 cm^3 per minute, to maximize the probability that CO_2 and N_2O are trapped as the non-condensable gases are pumped away. After about 5 min of regulating the flow with about 80 % of the air extracted, the valve is fully opened and sample extraction continues for an additional 15 min until about 99 % of the non-condensable gas has been removed (air pressure remaining about 0.05 Torr). The "w" shaped trap, with the liquid nitrogen only submerging the lower portion of the trap, effectively has two closely spaced "u" traps. This proved to be important for preventing the loss of CO_2 in the fast moving stream of air (for example by advecting flakes of frozen CO_2), without greatly decreasing the conductance of the

AMTD
7, 6529–6564, 2014

vacuum line. Though the cryocooler also showed promise as a residual air pump and the turbo-molecular pumping system ultimately proved more efficient at extracting the last few percent of sample without any significant isotopic fractionation.

With the CO_2 and N_2O held in the "w" trap, valves 7 and 12 are closed (Fig. 1) to isolate the sample from the portion of the extraction line exposed to water vapor. The "w" trap is warmed to 170 K by replacing the liquid nitrogen Dewar flask with a chilled ethanol-slush Dewar flask. This releases the CO_2 and N_2O but secures any water that may have passed through the primary water trap. The amount of CO_2 and N_2O is then is determined manometrically (MKS Baratron). The sample amount is used to predict the subsequent sample inlet pressure on the dual-inlet and pre-adjust the reference bellows accordingly. To transfer the now dry CO_2 and N_2O to the dual-inlet system, a small stainless steel tube attached to the line with a VCR fitted valve is immersed in liquid nitrogen for about 1 min, allowing the gases to condense in the tube. This tube is removed from the extraction line and attacbed to the sample side of the dual-inlet prior to analysis with a VCR copper sealed gasket.

3.3 Dual-Inlet IRMS measurement

The dual-inlet portion of the analysis is a computer controlled routine (Thermo Fisher Scientific, Inc.), modified slightly to accommodate the small samples and the measurement of the m/z 30 beam. The CO_2 and N_2O bypass the sample bellow and are condensed in a 150 µL cold finger known as the "micro-volume" for a period of 120 s. Valves are closed so that the microvolume bleeds only to the changeover valve via a crimped capillary. The microvolume is warmed to 28 °C to allow the CO_2 and N_2O to leak into the ion source.

With the reference side pre-adjusted to the expected sample size, the automated bellow adjustment period is typically minimal. Once the reference beam is within about 100 mV of the sample intensity, typically by the time the sample beam intensity is about 3000 mV, the reference side micro-volume (also 150 µL) is isolated from its bellow, and the dual-inlet measurement begins.

AMTD
7, 6529–6564, 2014

The operating range for the dual-inlet pressure was between about 0.01–0.015 bar, equivalent to a sample size of 1.5–2.25 bar µL CO_2. The measurement is comprised of eight dual-inlet cycles, each with an integration time of 8 s and idle time for changeover switching of 15 s. By the end of the measurement, the sample beam is typically 1000–2000 mV. A careful balance of the reference and sample capillary crimps and pre-adjustment of the reference bellows was required to keep the difference in m/z 44 beam intensity between the reference and sample beam both small and consistent (mean offset = 77 mV, 1-sigma standard deviation = 40 mV). After the CO_2 analysis is complete, the instrument jumps the major ion beam to m/z 30 and measures this intensity on the sample and reference beams. The ^{17}O abundance correction follows the formulation of Santrock et al. (1985). All traps are heated to about 50 °C and pumped before the start of the next analysis.

3.4 Calibration

In order to calibrate the isotopic values of the sample measurements, a working reference gas of pure CO_2 (Oztech) was measured on a daily basis against at least six aliquots of a NOAA standard air (hereafter: NOAA1). The "NOAA" standards were calibrated by the INSTAAR Stable Isotope Lab, University of Colorado to the VPDB-CO_2 scale with the primary reference as NBS-19 (isotopic values of all standards are in Table 2). The NOAA standard gas aliquots were processed with the sample extraction line both before and after the samples were analyzed. Typically, the mean of all six NOAA standard gas measurements was used as one-point calibration for the working reference gas. All the standard gas measurements, relative to a fixed working reference gas value are shown in Fig. 2.

Over the analysis period, the 1-sigma standard deviation of the NOAA1 standard was 0.03 and 0.13 ‰, for $\delta^{13}C$ and $\delta^{18}O$ respectively. However, the signal is not completely random, the $\delta^{13}C$ and $\delta^{18}O$ co-vary on the time frame of a few days (R^2 = 0.13; slope = 1.78; intercept = 7.42; p value < 0.01) (Fig. 2). Often, the standard gas appears to become more depleted, or alternatively, the working reference gas become more

AMTD
7, 6529–6564, 2014

enriched, by about 0.075 ‰ in $\delta^{13}C$ over the course of a few days, with the trend reversed when the working reference gas is replenished. This trend was confirmed during early experimentation and sample analysis by occasionally measuring the reference bellow against the same gas in the sample bellow that was only lightly consumed of the course of analysis. Assuming no leaks were present, this suggests that the gas in the reference bellows was becoming more enriched if not replenished frequently.

Reference gas enrichment over time may be at least partially due to a mass dependent distillation process operating as the gas in reference bellow is consumed. Because the amount of gas in the bellows has to be very small to accommodate the lower sample size (e.g. 10 mbar at 100 % expansion ≈ 0.25 mbar mL), the gas is quickly consumed over a few days of analysis, typically 10 % per day. Given Rayleigh distillation, this would roughly correspond to a fractionation factor of about 1 ‰ for $\delta^{13}C$ and 2 ‰ for $\delta^{18}O$. While much smaller than the expected $\delta^{13}C$ fractionation if molecular flow dominated the flow-regime (∼ 11 ‰) (Halsted and Nier, 1950), it does suggests the flow is not completely viscous at all times. Ultimately, the effect on precision of the sample measurements is negligible because the working reference gas is calibrated to the NOAA standard every day. From a practical standpoint, it requires that the working reference gas is replenished about every other day and gas consumption is minimized.

Additional experiments with a second NOAA standard (NOAA2) of similar $\delta^{13}C\text{-}CO_2$ (−8.106 ‰) but very different $\delta^{18}O\text{-}CO_2$ (−0.777 ‰), CO_2 (∼ 150 ppm) and N_2O (∼ 321 ppb), as well as another working reference gas with very different $\delta^{13}C$ (−3.58 ‰) were made to test the validity of a one-point calibration (see Table 2). The accuracy of the NOAA calibration scale was also checked by measuring the working reference gases against the carbonate standard NBS-19 with a Kiel Device, allowing for an independent in-house calibration of the NOAA standards (reported in Table 2). With the NOAA1 standard being measured over 400 times against the working reference, the INSTAAR-SIL and in-house calibration converge within 0.001 ‰ for $\delta^{13}C\text{-}CO_2$. The difference between the calibrations for the NOAA2 standard $\delta^{13}C\text{-}CO_2$ (0.034 ‰) is

AMTD
7, 6529–6564, 2014

probably a product of the significantly less frequent measurement of the NOAA2 standard, which was used almost exclusively to calibrate the N_2O measurement.

3.5 N_2O Measurement

To correct the IRMS measurements for the isobaric interference of N_2O, we employ a method that uses the fragmentation of N_2O in the source to estimate both the N_2O-to-CO_2 ratio and the ionization efficiency of N_2O (Assonov and Brenninkmeijer, 2006). The ion beam at m/z 30, composed primarily of $^{14}N^{16}O^+$ derived from N_2O and $^{12}C^{18}O^+$ derived from CO_2, is compared to the m/z 44 intensity in both the sample (a unknown mixture of N_2O and CO_2) and the reference (pure CO_2). The difference between m/z 30 signal of the sample and the reference is a measure of the N_2O in sample that is has been ionized in the source. The fragmentation yield of $^{14}N^{16}O^+$ from N_2O (^{30}Intensity/^{44}Intensity of $N_2O = {}^{30}$R-N_2O) and the ionization efficiency of N_2O (E-N_2O) must be determined in order to completely estimate the N_2O-to-CO_2 ratio. This technique differs from a previous method applied to ice core air which used the m/z 30-to-28 ratio (Friedli and Siegenthaler, 1988) which can be susceptible m/z 28 contamination by $^{14}N^{14}N^+$ from small leaks (Assonov and Brenninkmeijer, 2006).

Idealized experiments with pure N_2O and/or N_2O diluted in an inert gas can be performed to quantify these parameters. We calibrated the method using two NOAA calibrated standards with very different N_2O-to-CO_2 ratios (0.00091 and 0.00214) to estimate the two unknowns. Our initial calibration found effective values of ^{30}R-$N_2O = 0.19$ and E-$N_2O = 0.70$.

We report N_2O in terms of ppb, rather than the more cumbersome N_2O-to-CO_2 ratio that is directly measured. To calculate the N_2O and associated errors of the NOAA standard measurements in terms of ppb we use a constant CO_2 concentration known from the NOAA calibration. For the samples, we use the CO_2 concentration measured on our GC system, introducing a source of error from the offline analysis.

AMTD
7, 6529–6564, 2014

Because only the NOAA1 standard was analyzed on a day-to-day basis, only one single N_2O-to-CO_2 ratio was used to monitor the drift in the calibration, and occasionally make small adjustments. Generally the drift over the course of weeks was comparable to analytical uncertainty in the measurement (±1.7 ppb) (Fig. 3). However, following a re-tuning of the source parameters after 6 months of heavy use for unrelated experiments the calibration was observed to have changed significantly. Without the re-calibration using the two NOAA standard gases, the inferred N_2O would have been about 25 ppb lower than expected (see open squares in Fig. 3). The two-point calibration check is thus essential after any change in the source conditions or after many weeks of analysis.

The N_2O measurements from the ice core samples proved very effective with a sample reproducibility of ±4 ppb (1-sigma standard deviation, Table 1), an improvement on previous low-precision mass spectrometric methods and similar to that of gas chromatographic methods (Flückiger et al., 2004) and precise to about 5 % relative to the 80 ppb glacial-interglacial dynamic range (Schilt et al., 2010). The uncertainty in N_2O measurements from the isotopic fragment propagates into an uncertainty in the isobaric correction of ±0.0045 ‰ for $\delta^{13}C\text{-}CO_2$. Additionally, a comparison between the m/z 30 reconstruction and an independent N_2O record derived from an N_2O isotopic method on essentially the same samples from the Taylor Glacier archive shows an insignificant mean and 1-sigma standard deviation offset between the two records of only 1 ± 4 ppb (Schilt et al., 2014).

4 Method performance

4.1 Linearity

With a dual-inlet system, careful balancing of the capillaries and precise pressure adjustment mitigates most ion source non-linearity. During the periods of analysis, the linearity of the method is demonstrated by relationship between intensity and measured

AMTD
7, 6529–6564, 2014

δ^{13}C and δ^{18}O values relative to the working reference standard (Fig. 4). Because the gas for these standard measurements was passed through the gas extraction line, they offer a measure of the overall non-linearity of the system.

δ^{13}C-CO_2 increases modestly at about 0.021 ± 0.008 ‰ V^{-1} and δ^{18}O-O_2 shows very little trend relative to the noise at 0.003 ± 0.039 ‰ (Fig. 4). The standard error of a given measurement (i.e. internal precision) shows a slight trend towards decreased precision with smaller sample size (δ^{13}C-CO_2 s.e. = -0.0016 ‰ V^{-1}; δ^{18}O-CO_2 s.e. = -0.0042 ‰ V^{-1}; both about 20 % over mean s.e. per volt).

Because most measurements fell with a relatively narrow range of major beam intensities (~ 2000–3000 mV), no non-linearity correction was applied to the data. In the rare instance that the sample size was significantly less than expected (< 2000 mV) a series of standard measurements were completed in that range and a separate calibration for the sample was constructed.

4.2 Precision

Precision is estimated by performing replicate analyses on a selection of samples for the various archives. In the case of WDC05A, the sampling allows for true duplication, that is two samples from the same exact depth. Otherwise, as is the case with WDC06A and Taylor Glacier, duplicates are from adjacent depths (~ 20 cm between mid-depth). Given the degree of gas smoothing in the firn and the depth-age relationship at these sites, the adjacent depths should record nearly identical atmospheric values. For example, assuming a Gaussian gas age distribution with a full width at half maximum of at least 20 years and depth/age relationship about 20 cm year^{-1} at WAIS Divide (Mitchell, 2013) implies that two gas sample spaced 20 cms apart contain about 95 % of the same air. However, variability in the chemistry of the ice is present on these length scales (e.g. annual layers in WDC cores). Replicate analysis from adjacent depths for species that can be subject to in situ production in the ice, most notably of N_2O, could therefore artificially inflate apparent uncertainties.

AMTD
7, 6529–6564, 2014

The pooled standard deviation of all the δ^{13}C-CO_2 replicate analyses is 0.018 ‰ (n = 23) (Table 1). This is an improvement of at least 30 % on previous dual-inlet methods (reported range from 0.03 ‰ (Grater 1, n = 3) to 0.06 ‰ (Grater 6, n = 5) in Rubino et al., 2013), at least a 60 % improvement on the sublimation technique of Schmitt et al., 2011 (minimum ∼ 0.05 ‰) and nearly an order of magnitude better than most of the GC-IRMS techniques. Parsed by ice archive, the estimated precisions are very similar (Table 1) and an F test comparison of the variance in Taylor Glacier and WAIS Divide replicates reveals no statistically significant difference in precision ($p > 0.1$).

4.3 Accuracy

Evaluating the accuracy of ice core gas measurements is a significant challenge, primarily because it is impractical to manufacture an artificial ice sample with a known gas composition. As an alternative, we performed experiments in which a gas-free piece of ice (made in the laboratory) is grated along with an aliquot of known NOAA standard gas; this test examines accuracy after the release of occluded air from ice. When using a standard freezer capable of housing the ice grater at −25 °C, we found that standard gas became more depleted in δ^{13}C-CO_2 than expected when grating the ice or when the ice was warmed in the absence of any grating. This depletion, or "blank" appears to be proportional to the water vapor pressure after air extraction (and by inference the surface temperature of the ice block) (Fig. 5).

After obtaining an ultra-low temperature freezer operated at −60 °C, we were able to restrict the water vapor pressure to about 50 mTorr after grating. The reduction of water vapor raised the mean δ^{13}C-CO_2 value and decreased the scatter in blanks experiments to -0.066 ± 0.036 ‰ (1-sigma s.d. n = 12) though blanks of up to −0.11 ‰ were observed on vigorously grated ice blocks (Fig. 5). We could not differentiate by experiment whether this effect was dominated by the amount of the water vapor in the grater itself or the flux of water vapor from the ice grater into the extraction line. Based on these experiments we chose to correct all sample measurements assuming a constant

AMTD
7, 6529–6564, 2014

blank of +0.066 ‰. This can be compared to the results of Rubino et al. (2013) which observed blanks of -0.05 ± 0.02 ‰ ($n = 4$) and -0.11 ± 0.10 ‰ ($n = 15$) for graters 1 and 6, respectively. By propagating our sample reproducibility (±0.018 ‰) with the uncertainty in determining the procedural blank (±0.036 ‰) we estimate the accuracy of a single measurement to fall within ±0.04 ‰ (1-sigma s.d.) of the NOAA scale if these errors are uncorrelated. For comparison, the same metric would suggest that the Rubino et al. (2013) method should fall within ±0.036 and ±0.12 ‰ of the CSIRO scale for grater 1 and 6, respectively.

5 Oxygen isotopic fractionation

The oxygen isotopic composition of atmospheric CO_2 is primarily controlled by the exchange of oxygen between CO_2 and H_2O during photosynthesis in plant leaves and respiration in soils. Atmospheric δ^{18}O-CO_2 therefore offers a constraint on gross of primary production and the hydrological cycle on a global scale (Welp et al., 2011). However, the atmospheric signal of δ^{18}O-CO_2 in ice core gas is probably compromised by exchange of oxygen with the surrounding ice (Friedli et al., 1984). The process by which this exchange occurs is somewhat enigmatic as it most likely requires the interaction of CO_2 and liquid water at sub-freezing temperatures. Though liquid water in very small amounts is probably ubiquitous in polar ice, specifically at the triple junctions of grains (Mader, 1992; Nye and Frank, 1973), its influence on the preservation of gas records is not well known. A better understanding of the interaction of gas and ice is important for constraining any possible diffusion of atmospheric signals in the very old (> 1 million years ago) and very warm basal ice that may be recovered as part of "Oldest Ice" project (Fischer et al., 2013).

Observations of ice core δ^{18}O-CO_2 have previously been reported and discussed from low-resolution measurements from ice cores at Siple Dome, South Pole and Byrd (Siegenthaler et al., 1988; hereafter Siegenthaler) and high-precision measurements from firn sampling campaigns at Dome C, Dronning Maud Land, and Berkner Island

AMTD
7, 6529–6564, 2014

(Assonov et al., 2005; hereafter ABJ). Siegenthaler observed δ^{18}O-CO_2 values about 20 to 30 ‰ more depleted than typical atmospheric values and correlated to the variations of δ^{18}O in the surrounding ice matrix. ABJ also observed δ^{18}O-CO_2 becoming more depleted relative to the atmosphere as the age of the CO_2 increases with depth in the firn.

We too observe very highly correlated δ^{18}O-CO_2 and δ^{18}O-H_2O (Figs. 6 and 7). Most notably, the high (~ 3 cm) resolution δ^{18}O-H_2O data from the WDC05A core (Steig et al., 2013) allows us to accurately determine the mean δ^{18}O surrounding each gas sample (Fig. 6). δ^{18}O-H_2O measurements from Taylor Glacier (D. Baggenstos, personal communication, 2013) are only available in nearby samples so the δ^{18}O-H_2O data was smoothed and interpolated before comparison with the gas data. The apparent fractionation (ε) between CO_2 and H_2O is determined by taking the difference between δ^{18}O-CO_2 and δ^{18}O-H_2O on a sample-by-sample basis. Note that $\varepsilon_{a-b} = 1000 \ln(\alpha_{a-b}) \approx \delta_a - \delta_b$.

The mean and 1-sigma standard deviation of the apparent ε (CO_2-$H_2O_{(s)}$) is 47.43 ± 0.45 and 44.42 ± 1.34 ‰, for WDC05A and Taylor Glacier, respectively (Table 3). With the in situ ice temperature of WDC05A about 11 K colder than Taylor Glacier, there appears to be an increase in fractionation with decreasing temperature. The higher noise in the Taylor Glacier δ^{18}O-CO_2 data is probably related to the aliasing of high-frequency δ^{18}O-H_2O variability.

The ε (CO_2-$H_2O_{(s)}$) show no discernible trend with time. Even the youngest sample at WAIS Divide (gas age = 1915 C.E.) is only about 1 ‰ heavier than the mean ε (CO_2-$H_2O_{(s)}$) for the entire core, appearing to be mostly equilibrated with the surrounding ice. This is consistent with the observation of the rate of exchange in the firn. ABJ calculate the equilibration proceeds with a half-life of about 23 years at the Berkner Island Site, which at −26 °C is only slightly warmer than WAIS Divide, suggesting that youngest WAIS Divide sample should be about 90 % equilibrated.

Siegenthaler proposed that apparent fractionation between the ice matrix and gaseous CO_2, could be described by temperature dependent fractionation at

AMTD
7, 6529–6564, 2014

thermodynamic equilibrium between gaseous CO_2 and the solid, liquid and vapor phases of the H_2O as follows:

$$\alpha(CO_2 - H_2O_{(s)}) = \alpha(CO_2 - H_2O_{(l)})\alpha(H_2O_{(l)} - H_2O_{(g)})\alpha(H_2O_{(g)} - H_2O_{(s)}) \quad (1)$$

The left hand side of the equation is the expected fractionation between gaseous CO_2 and solid water – what we would expect to see in the ice core. The fractionation factors on the right hand side of the equation have been estimated by theoretical and experimental work, but α (CO_2-$H_2O_{(l)}$) and α ($H_2O_{(l)}$-$H_2O_{(g)}$) have not been determined below the freezing point of water. The α ($H_2O_{(g)}$-$H_2O_{(s)}$) has been determined over a wide range of sub-freezing temperatures because of its relevance in interpreting oxygen isotope records from polar ice but is not well-constrained at very cold temperatures ($\sim < 240$ K).

Siegenthaler used α (CO_2-$H_2O_{(l)}$) from Bottinja (1968) and α ($H_2O_{(l)}$-$H_2O_{(g)}$) and α ($H_2O_{(g)}$-$H_2O_{(s)}$) from Majoube (1971) (Table 4 summarizes these and other fractionation factors, and provides shorthand for the formulations). Using the fractionation factors from Siegenthaler, we find our δ^{18}O-CO_2 values are 1.19 ± 0.45 and 1.58 ± 1.34 ‰ more depleted than would be expected from complete equilibration in WAIS Divide and Taylor Glacier, respectively (Table 3). Given the uncertainties is determining the apparent fractionation from the noisy data and accurately measuring δ^{18}O-CO_2, the new data are mostly in agreement with previous data and proposed model for δ^{18}O-CO_2 equilibration (Fig. 8).

The uncertainties in the ice core data, however, are smaller than the uncertainties in other experimentally and theoretically derived estimates of temperature dependent fractionation. Including additional estimates suggests that the predicted α (CO_2-$H_2O_{(s)}$) is relatively insensitive to changing α (CO_2-$H_2O_{(l)}$) and α ($H_2O_{(l)}$-$H_2O_{(g)}$) (black band, Fig. 8). However, the convergence of the expected fractionation from various studies does not necessarily equate to accuracy because these formulations are extrapolated below the freezing point. On the other hand, α (CO_2-$H_2O_{(s)}$) appears very sensitive to different α ($H_2O_{(g)}$-$H_2O_{(s)}$) predictions from experimental observations (Ellehoj et al.,

AMTD
7, 6529–6564, 2014

2013; Majoube, 1971) and theoretical work (Méheut et al., 2007), showing a divergence at very cold temperatures (dot and dash-dot lines, Fig. 8) that is larger than the error in the ice core measurements. Though α ($H_2O_{(g)}$-$H_2O_{(s)}$) can probably be better constrained by controlled experiments in the laboratory, ice core δ^{18}O-CO_2 may offer a unique, natural experiment to observe this process over long time periods, warranting further work.

Finally, by combining our data with the results from Siegenthaler, we derive a relationship for α (CO_2-$H_2O_{(s)}$) and temperature with the form:

$$\varepsilon = 1000\ln(\alpha) = \frac{K_2(10^6)}{T^2} - \frac{K_1(10^3)}{T} + K_0 \quad (2)$$

With temperature in absolute degrees, $K_2 = 19.5 \pm 27.6$, $K_2 = -145 \pm 226$ and $K_0 = 312 \pm 461$. The relationship remains under constrained (light grey band in Fig. 8 shows 95 % C.I. of the fit). Additional data from ice archives with different temperature, especially at sites with very cold temperatures, would narrow the uncertainty in these coefficients.

6 Conclusions

The method presented here advances the methodology for measuring the δ^{13}C-CO_2 from polar ice. The external precision of ±0.018 ‰ and accuracy of ±0.04 ‰ obtained by dual-inlet mass spectrometry is an improvement on most other methods. To put this some perspective, this method can resolve isotopic variations of about 6 % of the total glacial-interglacial range of δ^{13}C-CO_2 (~ 0.3 ‰), which is essential for understanding carbon cycle dynamics. Also, very fast inputs of terrestrial carbon to the atmosphere (signature of about ~-0.03 ‰ ppm^{-1} CO_2) can be delineated for CO_2 variations of less than 3 ppm.

This study describes the rigorous testing and careful analytical procedures, including source tuning, linearity testing, and daily calibration that are required to obtain

AMTD
7, 6529–6564, 2014

high-precision with a dual-inlet technique on very small samples (~ 1.5 bar µL). By demonstrating a method for accurately correcting for isobaric interference of N_2O on small sample, a significant barrier for dual-inlet measurement of ice core or other limited atmospheric sampling studies of CO_2 has been surmounted. Our dual-inlet method provides a means for determining the CO_2 and N_2O mixing ratios on the same ancient air sample, given sufficiently large ice samples. Finally, the $\delta^{18}O$-CO_2 data presented here constrain the fractionation of oxygen isotopes during what appears to be an exchange of oxygen between CO_2 and solid ice. Future methodological improvements should focus on increasing the grating efficiency to make the method suitable for clathrated ice.

Acknowledgements. This work was supported by NSF Grant 0839078 (EJB and ACM). Oregon State University provided additional support for mass spectrometer purchase and management of the OSU/CEOAS stable isotope laboratory. We thank the WAIS Divide Science Coordination Office for the collection and distribution of the WAIS Divide ice core (Kendrick Taylor (Desert Research Institute of Reno Nevada), NSF Grants 0230396, 0440817, 0944348; and 0944266 – University of New Hampshire) and the Taylor Glacier 2010–2011 Field Team (Daniel Baggenstos, James Lee, Hinrich Schaefer, Tanner Kuhl, Robb Kulin, Jeff Severinghaus, Vas Petrenko and Paul Rose) for collection of Taylor Glacier samples with support from NSF Grant 0838936 (EJB). We also appreciate comments provided by R. H. Rhodes on an earlier version of this manuscript.

References

Ahn, J., Brook, E. J., and Howell, K.: A high-precision method for measurement of paleoatmospheric CO_2 in small polar ice samples, J. Glaciol., 55, 499–506, 2009.

Assonov, S. S. and Brenninkmeijer, C. A. M.: On the N_2O correction used for mass spectrometric analysis of atmospheric CO_2, Rapid Commun. Mass Sp., 20, 1809–1819, doi:10.1002/rcm.2516, 2006.

Assonov, S. S., Brenninkmeijer, C. A. M., and Jöckel, P.: The ^{18}O isotope exchange rate between firn air CO_2 and the firn matrix at three Antarctic sites, J. Geophys. Res.-Atmos., 110, D18310, doi:10.1029/2005JD005769, 2005.

AMTD
7, 6529–6564, 2014

Bottinga, Y. and Craig, H.: Oxygen isotope fractionation between CO_2 and water, and the isotopic composition of marine atmospheric CO_2, Earth Planet. Sc. Lett., 5, 285–295, 1968.

Brenninkmeijer, C. A. M., Kraft, P., and Mook, W. G.: Oxygen Isotope Fractionation Between CO_2 and H_2O, Isot. Geosci., 1, 181–190, 1983.

Ellehoj, M. D., Steen-Larsen, H. C., Johnsen, S. J., and Madsen, M. B.: Ice-vapor equilibrium fractionation factor of hydrogen and oxygen isotopes: Experimental investigations and implications for stable water isotope studies, Rapid Commun. Mass Sp., 27, 2149–2158, doi:10.1002/rcm.6668, 2013.

Elsig, J., Schmitt, J., Leuenberger, D., Schneider, R., Eyer, M., Leuenberger, M., Joos, F., Fischer, H., and Stocker, T. F.: Stable isotope constraints on Holocene carbon cycle changes from an Antarctic ice core, Nature, 461, 507–510, doi:10.1038/nature08393, 2009.

Fischer, H., Severinghaus, J., Brook, E., Wolff, E., Albert, M., Alemany, O., Arthern, R., Bentley, C., Blankenship, D., Chappellaz, J., Creyts, T., Dahl-Jensen, D., Dinn, M., Frezzotti, M., Fujita, S., Gallee, H., Hindmarsh, R., Hudspeth, D., Jugie, G., Kawamura, K., Lipenkov, V., Miller, H., Mulvaney, R., Pattyn, F., Ritz, C., Schwander, J., Steinhage, D., van Ommen, T., and Wilhelms, F.: Where to find 1.5 million yr old ice for the IPICS "Oldest Ice" ice core, Clim. Past Discuss., 9, 2771–2815, doi:10.5194/cpd-9-2771-2013, 2013.

Flückiger, J., Blunier, T., Stauffer, B., Chappellaz, M., Spahni, R., Kawamura, K., Schwander, J., Stocker, T. F., and Dahl-Jensen, D.: N_2O and CH_4 variations during the last glacial epoch: insight into global processes, Global Biogeochem. Cy., 18, GB1020, doi:10.1029/2003GB002122, 2004.

Francey, R. J., Allison, C. E., Etheridge, D. M., Trudinger, C. M., Enting, I. G., Leuenberger, M., Langenfelds, R. L., Michel, E., and Steele, L. P.: A 1000-year high precision record of $\delta^{13}C$ in atmospheric CO_2, Tellus B, 51, 170–193, doi:10.1034/j.1600-0889.1999.t01-1-00005.x, 1999.

Friedli, H. and Siegenthaler, U.: Influence of N_2O on isotope analyses in CO_2 and mass-spectrometric determination of N_2O in air samples, Tellus B, 40, 129–133, doi:10.1111/j.1600-0889.1988.tb00216.x, 1988.

Friedli, H. and Stauffer, B.: Ice core record of the $^{13}C/^{12}C$ ratio of atmospheric CO_2, in the past two centuries, Nature, 324, 237–238, 1986.

Friedli, H., Moor, E., Oeschger, H., Siegenthaler, U., and Stauffer, B.: 13C/12C ratios in CO_2 extracted from Antarctic ice, Geophys. Res. Lett., 11, 1145–1148, doi:10.1029/GL011i011p01145, 1984.

AMTD
7, 6529–6564, 2014

Halsted, R. E. and Nier, A. O.: Gas Flow through the Mass Spectrometer Viscous Leak, Rev. Sci. Instrum., 21, 1019–1021, doi:10.1063/1.1745483, 1950.

Horita, J. and Wesolowski, D. J.: Liquid–vapor fractionation of oxygen and hydrogen isotopes of water from the freezing to the critical temperature, Geochim. Cosmochim. Ac., 58, 3425–3437, 1994.

Indermuhle, A., Stocker, T. F., Joos, F., Fischer, H., Smith, H. J., Wahlen, M., Deck, B., Mastroianni, D., Tschumi, J., Blunier, T., Meyer, R., and Stauffer, B.: Holocene carbon-cycle dynamics based on CO_2 trapped in ice at Taylor Dome, Antarctica, Nature, 398, 121–126, 1999.

Leuenberger, M., Siegenthaler, U., and Langway, C. C.: Carbon isotope compositoin of atmospheric CO_2 during the last ice-age from an Antarctic ice core, Nature, 357, 488–490, 1992.

Leuenberger, M. C., Eyer, M., Nyfeler, P., Stauffer, B., and Stocker, T. F.: High-resolution delta C-13 measurements on ancient air extracted from less than 10 cm(3) of ice, Tellus B, 55, 138–144, 2003.

Lourantou, A., Lavric, J. V., Kohler, P., Barnola, J. M., Paillard, D., Michel, E., Raynaud, D., and Chappellaz, J.: Constraint of the CO_2 rise by new atmospheric carbon isotopic measurements during the last deglaciation, Global Biogeochem. Cy., 24, GB2015, doi:10.1029/2009gb003545, 2010.

Mader, H. M.: Observations of the water-vein system in polycrystalline ice, J. Glaciol., 38, 333–347, 1992.

Majoube, M.: Oxygen-18 and deuterium fractionation between water and steam, J. Chim. Phys. Phys.-Chim. Biol., 68, 1423–1436, 1971.

Masarie, K. A., Langenfelds, R. L., Allison, C. E., Conway, T. J., Dlugokencky, E. J., Francey, R. J., Novelli, P. C., Steele, L. P., Tans, P. P., Vaughn, B., and White, J. W. C.: NOAA/CSIRO flask air intercomparison experiment: a strategy for directly assessing consistency among atmospheric measurements made by independent laboratories, J. Geophys. Res.-Atmos., 106, 20445–20464, doi:10.1029/2000JD000023, 2001.

Méheut, M., Lazzeri, M., Balan, E., and Mauri, F.: Equilibrium isotopic fractionation in the kaolinite, quartz, water system: prediction from first-principles density-functional theory, Geochim. Cosmochim. Ac., 71, 3170–3181, doi:10.1016/j.gca.2007.04.012, 2007.

Mitchell, L. E.: The Late Holocene Atmospheric Methane Budget Reconstructed from Ice Cores, Oregon State University, Corvallis, OR, Winter, 2013.

AMTD
7, 6529–6564, 2014

Mitchell, L. E., Brook, E. J., Sowers, T., McConnell, J. R., and Taylor, K.: Multidecadal variability of atmospheric methane, 1000–1800 CE, J. Geophys. Res.-Biogeo., 116, G02007, doi:10.1029/2010jg001441, 2011.

Miteva, V., Sowers, T., and Brenchley, J.: Production of N_2O by ammonia oxidizing bacteria at subfreezing temperatures as a model for assessing the N_2O anomalies in the Vostok Ice Core, Geomicrobiol. J., 24, 451–459, doi:10.1080/01490450701437693, 2007.

Nye, J. F. and Frank, F. C.: Hydrology of the intergranular veins in a temperate glacier, in: Symposium on the Hydrology of Glaciers, Vol. 95, 157–161, 1973.

Rubino, M., Etheridge, D. M., Trudinger, C. M., Allison, C. E., Battle, M. O., Langenfelds, R. L., Steele, L. P., Curran, M., Bender, M., White, J. W. C., Jenk, T. M., Blunier, T., and Francey, R. J.: A revised 1000 year atmospheric δ^{13}C-CO_2 record from Law Dome and South Pole, Antarctica, J. Geophys. Res.-Atmos., 118, 8482–8499, doi:10.1002/jgrd.50668, 2013.

Santrock, J., Studley, S. A., and Hayes, J. M.: Isotopic analyses based on the mass-spectrum of carbon-dioxide, Anal. Chem., 57, 1444–1448, doi:10.1021/ac00284a060, 1985.

Schaefer, H., Lourantou, A., Chappellaz, J., Lüthi, D., Bereiter, B., and Barnola, J.-M.: On the suitability of partially clathrated ice for analysis of concentration and δ^{13}C of palaeoatmospheric CO_2, Earth Planet. Sc. Lett., 307, 334–340, doi:10.1016/j.epsl.2011.05.007, 2011.

Schilt, A., Baumgartner, M., Blunier, T., Schwander, J., Spahni, R., Fischer, H., and Stocker, T. F.: Glacial–interglacial and millennial-scale variations in the atmospheric nitrous oxide concentration during the last 800 000 years, Clim. Last Million Years New Insights EPICA Rec., 29, 182–192, doi:10.1016/j.quascirev.2009.03.011, 2010.

Schilt, A., Brook, E. J., Bauska, T. K., Baggenstos, D., Fischer, H., Joos, F., Petrenko, V. V., Schaefer, H., Schmitt, J., Severinghaus, J. P., Spahni, R., and Stocker, T. F.: Isotopic constraints on marine and terrstrial N_2O emissions during the last deglaciation, Nature, in review, 2014.

Schmitt, J., Schneider, R., and Fischer, H.: A sublimation technique for high-precision measurements of $\delta^{13}CO_2$ and mixing ratios of CO_2 and N_2O from air trapped in ice cores, Atmos. Meas. Tech., 4, 1445–1461, doi:10.5194/amt-4-1445-2011, 2011.

Schmitt, J., Schneider, R., Elsig, J., Leuenberger, D., Lourantou, A., Chappellaz, J., Koehler, P., Joos, F., Stocker, T. F., Leuenberger, M., and Fischer, H.: Carbon isotope constraints on the deglacial CO_2 rise from ice cores, Science, 336, 711–714, doi:10.1126/science.1217161, 2012.

AMTD
7, 6529–6564, 2014

Siegenthaler, U., Friedli, H., Loetscher, H., Moor, E., Neftel, A., Oeschger, H., and Stauffer, B.: Stable-isotope ratios and concentration of CO_2 in air from polar ice cores, Ann. Glaciol., 10, 151–156, 1988.

Smith, H. J., Fischer, H., Wahlen, M., Mastroianni, D., and Deck, B.: Dual modes of the carbon cycle since the Last Glacial Maximum, Nature, 400, 248–250, 1999.

Steig, E. J., Ding, Q., White, J. W. C., Kuettel, M., Rupper, S. B., Neumann, T. A., Neff, P. D., Gallant, A. J. E., Mayewski, P. A., Taylor, K. C., Hoffmann, G., Dixon, D. A., Schoenemann, S. W., Markle, B. R., Fudge, T. J., Schneider, D. P., Schauer, A. J., Teel, R. P., Vaughn, B. H., Burgener, L., Williams, J., and Korotkikh, E.: Recent climate and ice-sheet changes in West Antarctica compared with the past 2000 years, Nat. Geosci., 6, 372–375, doi:10.1038/NGEO1778, 2013.

Trudinger, C. M., Enting, I. G., Rayner, P. J., and Francey, R. J.: Kalman filter analysis of ice core data – 2. Double deconvolution of CO_2 and delta C-13 measurements, J. Geophys. Res.-Atmos., 107, 4423, doi:10.1029/2001jd001112, 2002.

Welp, L. R., Keeling, R. F., Meijer, H. A. J., Bollenbacher, A. F., Piper, S. C., Yoshimura, K., Francey, R. J., Allison, C. E., and Wahlen, M.: Interannual variability in the oxygen isotopes of atmospheric CO_2 driven by El Nino, Nature, 477, 579–582, 2011.

Zhao, C. L., Tans, P. P., and Thoning, K. W.: A high precision manometric system for absolute calibrations of CO_2 in dry air, J. Geophys. Res.-Atmos., 102, 5885–5894, doi:10.1029/96jd03764, 1997.

AMTD
7, 6529–6564, 2014

Table 1. Ice archives utilized in this study with their respective precisions from replicate analysis.

				1-sigma pooled standard deviation of replicate analyses		
Ice Archive	Drill Fluid	Type of Replicates	*n*	δ^{13}C-CO_2 (‰)	CO_2 (ppm)	N_2O (ppb)
WDC05A	none	true	8	0.016	2.18	3.83
WDC06A	Isopar-K, HCFC-141b	adjacent depths	6	0.014	1.04	2.4
Taylor Glacier	none	adjacent depths	9	0.022	1.3	5.23
Overall			23	0.018	1.9	4.35

AMTD
7, 6529–6564, 2014

Table 2. Gas concentrations and nominal isotopic composition of reference gases.

	Mixing Ratio			Isotopic Composition			
	Reference Scale	CO_2 (ppm) (s.d)	N_2O (ppb) (s.d)	Analysis Facility	Primary Ref. Material	$\delta^{13}C\text{-}CO_2$ (VPDB-CO_2)	$\delta^{18}O\text{-}CO_2$ (VPDB-CO_2)
NOAA1	2007 WMO MOLE FRACTION	277.04 (0.03)	252.6 (0.2)	INSTAAR-SIL OSU	NBS-19 NBS-19	−8.288 −8.287	−7.171 −7.58
NOAA2	SCALE (CO_2), NOAA-2006 (N_2O)	150.01 (0.01)	321.96 (0.2)	INSTAAR-SIL OSU	NBS-19 NBS-19	−8.135 −8.101	−0.578 −0.934
Working Ref.	n.a.	pure	n.a.	Oztech OSU	 NBS-19	−10.39 −10.51	−9.84 −10.06

AMTD
7, 6529–6564, 2014

Table 3. Observed $\delta^{18}O$ of CO_2 fractionation results from this study and other studies.

Core	Study	Age Interval	$\delta^{18}O$-CO_2 (VPD-CO_2)	$\delta^{18}O$-H_2O (VPD-CO_2)	Temp. (K)	εCO_2-H_2O (Observed)
WAIS Divide	this study	1.25–0.1 ka	−25.17	−72.41	243	47.43 ± 0.45
Taylor Glacier		23–11 ka	−35.58	−80.00	254	44.42 ± 1.34
Siple Dome	(Siegenthaler et al., 1988)	0.3–0.1 ka	−20.40	−67.86	249	47.46
South Pole		0.9–0.4 ka	−31.70	−88.31	222	56.61
Byrd		~ 50 ka	−31.80	−78.23	238	46.43

AMTD
7, 6529–6564, 2014

Table 4. $\delta^{18}O$ fractionation factors.

$\alpha(A-B)$	$1000\ln(\alpha) =$	Reference	Short-hand
α (CO_2-$H_2O_{(l)}$)	$-\frac{0.021(10^6)}{T^2}+\frac{17.99(10^3)}{T-19.97}$	Bottinga and Craig (1968)	B68
	$\frac{17.6(10^3)}{T}-17.93$	Brenninkmeijer et al. (1983)	B83
α ($H_2O_{(l)}$-$H_2O_{(g)}$)	$\frac{1.137(10^6)}{T^2}-\frac{0.42(10^3)}{T}-2.07$	Majoube (1971)	M71
	$\frac{0.35(10^9)}{T^3}-\frac{1.666(10^6)}{T^2}+\frac{6.71(10^3)}{T}-7.68$	Horita and Wesolowski (1994)	HW94
α ($H_2O_{(s)}$-$H_2O_{(g)}$)	$\frac{11.84(10^3)}{T}-28.22$	Majoube (1971)	M71
	$-0.0016799x^3-0.00721x^2+1.675x-2.685$ where $x=\frac{10^6}{T^2}$	Méheut et al. (2007)	M07
	$\left(\frac{8312.5}{T^2}-\frac{49.192}{T}+0.0831\right)\times 1000$	Ellehoj et al. (2013)	E13

AMTD
7, 6529–6564, 2014

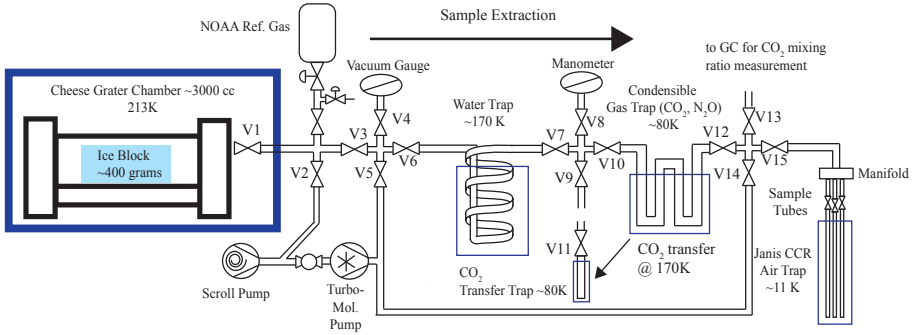

Figure 1. Extraction line. A simplified schematic of the ice core air extraction vacuum line.

AMTD
7, 6529–6564, 2014

Stable isotopes of CO_2 and the N_2O/CO_2 ratio of polar ice

T. K. Bauska et al.

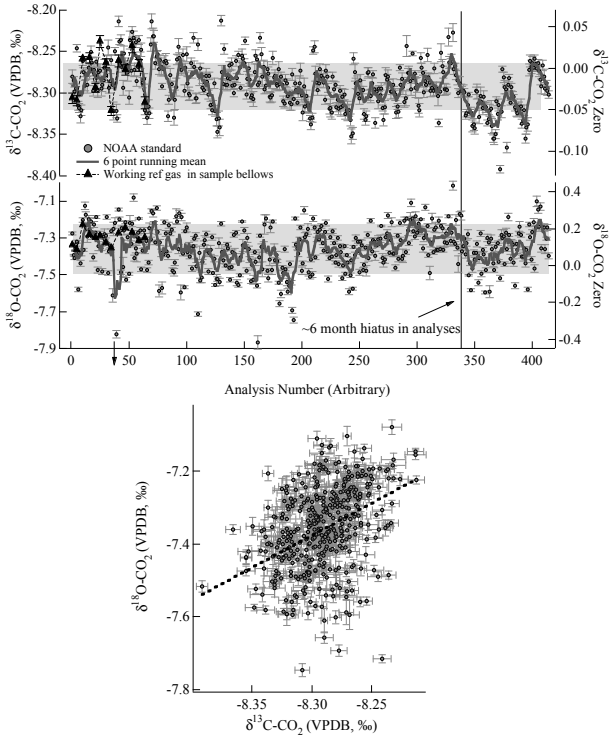

Figure 2. Standard measurement reproducibility. Upper panel: all measurements of the NOAA1 standard gas over the course of a number of measurement campaigns encompassing about 5 months time in total. The $\delta^{13}C$ and $\delta^{18}O\text{-}CO_2$ are reported relative to the working reference gas. Analyses of the working reference gas stored in the sample bellows (black triangles) (plotted on the "zero" axis). The gray bars represent the 1-sigma standard deviation of the NOAA1 standard over the entire period. Lower panel: $\delta^{13}C\text{-}CO_2$ covariation with $\delta^{18}O\text{-}CO_2$ (R^2 = 0.13).

AMTD
7, 6529–6564, 2014

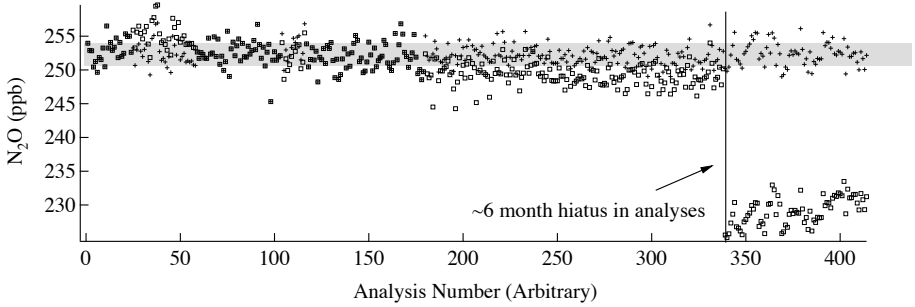

Figure 3. N_2O standard reproducibility. The reproducibility and drift in the N_2O calibration of the same period of analysis as in Fig. 2. The black crosses are the N_2O of the NOAA1 standard as determined by the daily calibration. The open squares represent the same data if the calibration was fixed to a set value at the beginning of analysis (time 0). This shows both a small drift from about number 0 to 300 ($\sim$ 4 months) and a major shift in the values around 340, which represents a 6 month hiatus and re-tuning of the ion source.

AMTD
7, 6529–6564, 2014

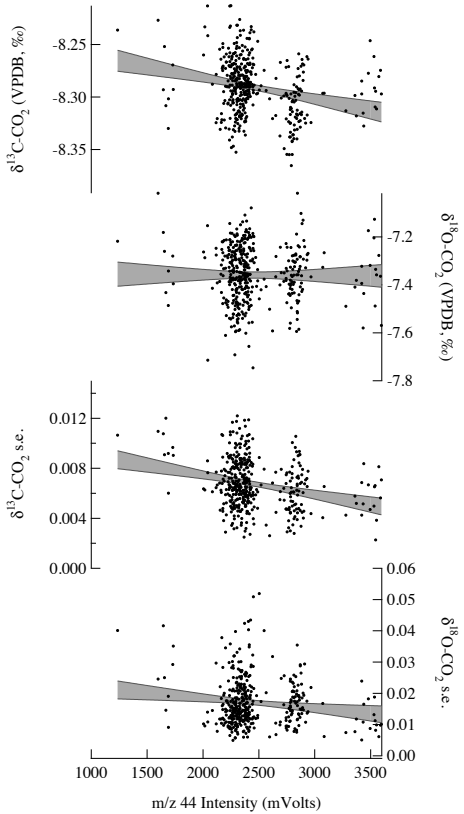

Figure 4. Linearity and precision of standard measurements. The linearity and internal precision of the measurement vs. m/z 44 intensity as recorded by measurements of the NOAA1 standard during the period of analysis. δ^{13}C and δ^{18}O-CO_2 are reported relative to the working reference gas (upper two panels) and the internal precision is reported as 1-sigma standard error of the eight dual-inlet measurements (lower two panels). The grey shading represents the 95 % confidence intervals for a linear fit to the data.

AMTD
7, 6529–6564, 2014

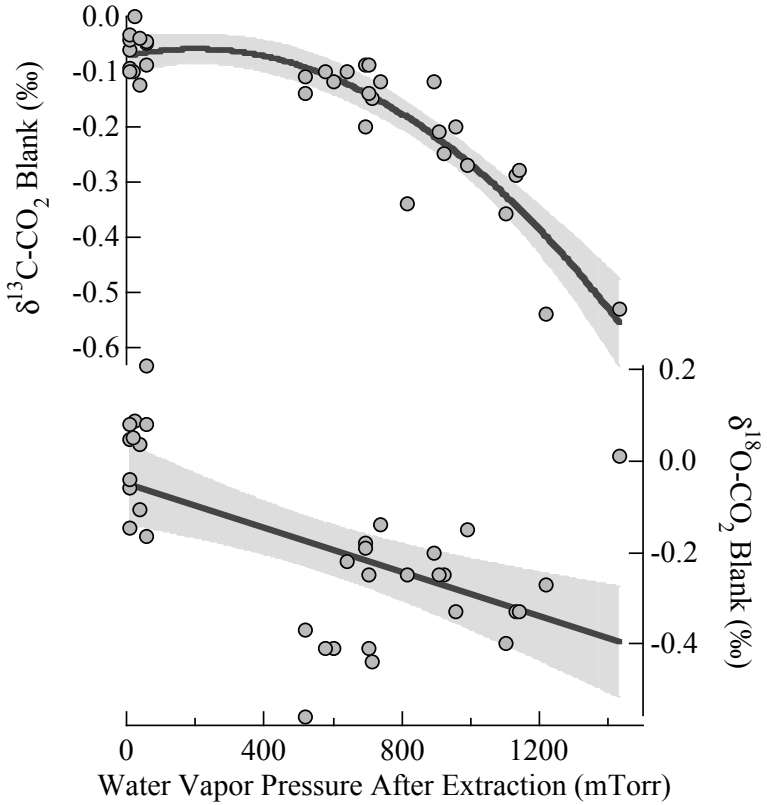

Figure 5. Procedural blank experiments. Measurements of the procedural blank of the system and its relationship to water vapor pressure. Blank is reported as the difference of the expected δ-value (from the NOAA calibration) to the measured value when ice grating and air extraction is simulated. Negative blanks indicate that the standard air become more negative during the simulation. The grey shading indicates 3rd order polynomial fit to the $\delta^{13}C\text{-}CO_2$ with 95 % confidence intervals and linear fit to the $\delta^{18}O\text{-}CO_2$.

AMTD
7, 6529–6564, 2014

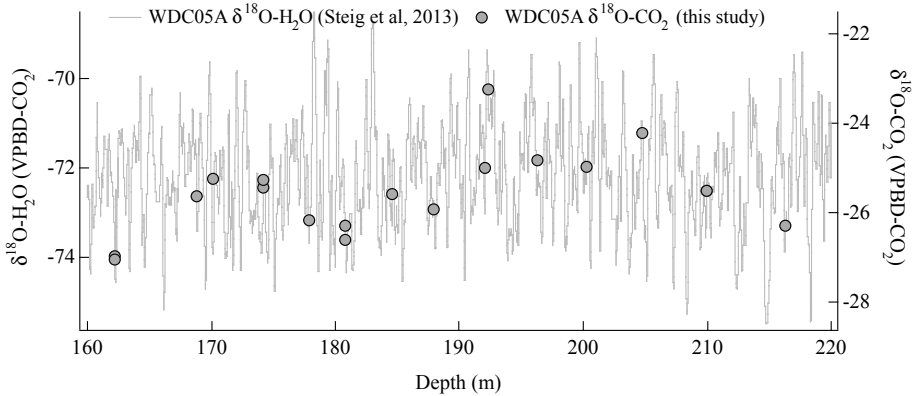

Figure 6. WAIS divide δ^{18}O-CO_2 and δ^{18}O-H_2O. A short selection of the δ^{18}O-CO_2 (this study) and δ^{18}O-H_2O data (Steig et al., 2013) on the depth scale from the WDC05A core. The two vertical axes are of the same magnitude but offset to show the ability of δ^{18}O-CO_2 to capture and integrate the fine scale δ^{18}O-H_2O.

AMTD
7, 6529–6564, 2014

Stable isotopes of CO_2 and the N_2O/CO_2 ratio of polar ice

T. K. Bauska et al.

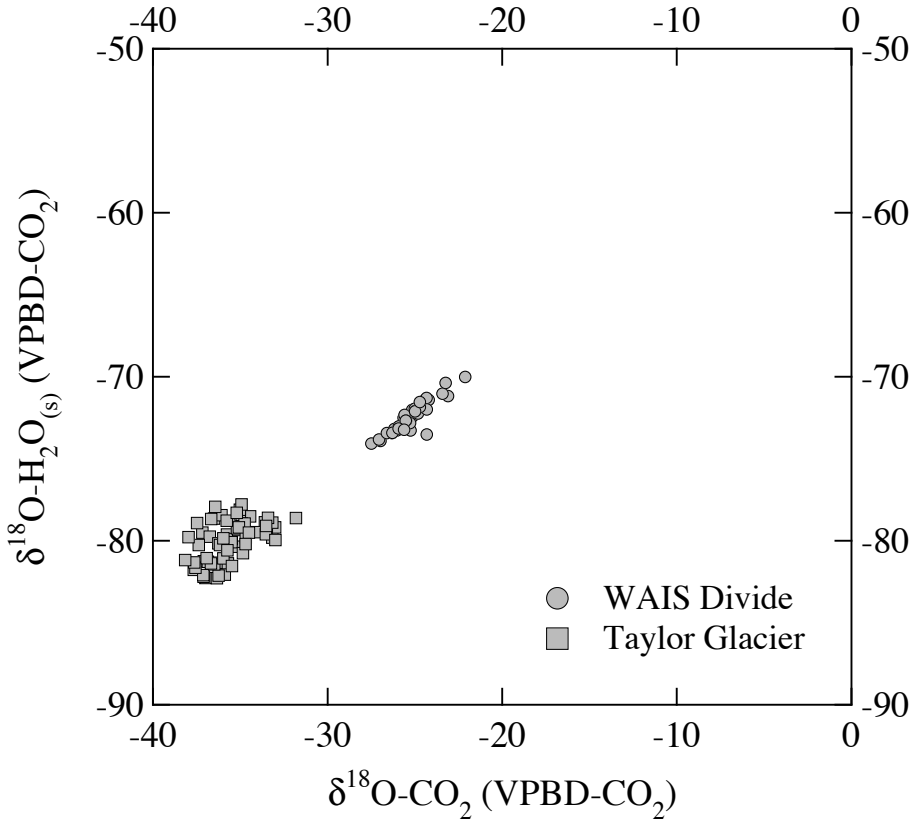

Figure 7. δ^{18}O-CO_2 and δ^{18}O-H_2O correlation. δ^{18}O-CO_2 plotted against δ^{18}O-H_2O from the WAIS Divide and Taylor Glacier archives.

AMTD
7, 6529–6564, 2014

Stable isotopes of CO_2 and the N_2O/CO_2 ratio of polar ice

T. K. Bauska et al.

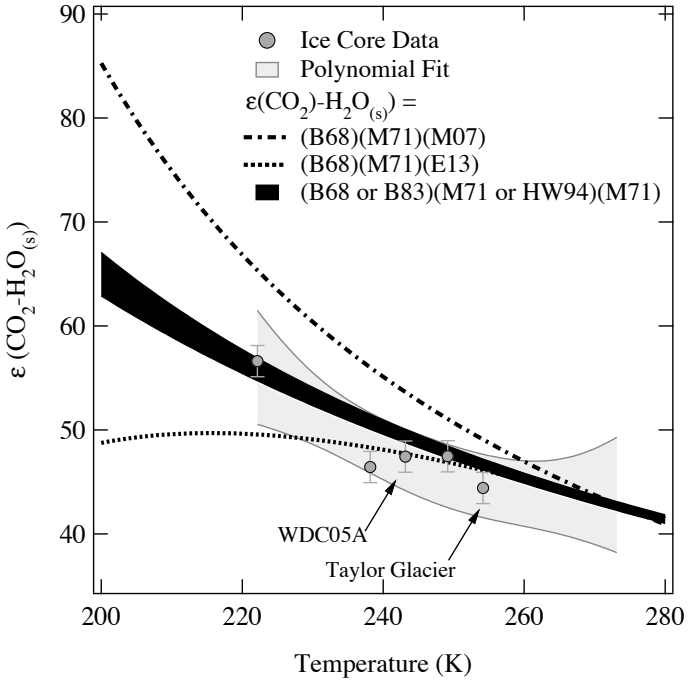

Figure 8. Temperature dependence of oxygen isotope fractionation. The relationship between ice core δ^{18}O-CO_2 gas fractionation ε (CO_2-$H_2O_{(s)}$) (grey circles) from this study (indicated with arrows) and Siegenthaler et al., 1988. The light grey shading indicates a 3rd order polynomial fit to the data. The curves indicated the predicated fraction in thermodynamic equilibrium of gaseous CO_2 with vapor, liquid and solid H_2O (Eq. 1). The black banding uses a range of determinations for α (CO_2-$H_2O_{(l)}$) and α ($H_2O_{(l)}$-$H_2O_{(g)}$) but only M71 for α ($H_2O_{(g)}$-$H_2O_{(s)}$). The dot-dashed line uses only B68 for α (CO_2-$H_2O_{(l)}$) and M71 for α ($H_2O_{(l)}$-$H_2O_{(g)}$) but M07 for α ($H_2O_{(g)}$-$H_2O_{(s)}$). The doted line also uses only B68 for α (CO_2-$H_2O_{(l)}$) and M71 for α ($H_2O_{(l)}$-$H_2O_{(g)}$) but E13 for α ($H_2O_{(g)}$-$H_2O_{(s)}$) (see Table 4 for a description of the fractionation formulas).

AMTD
7, 6529–6564, 2014